Quantum-stochasticity-induced asymmetry in the angular distribution of electrons in a quasiclassical regime

Guang Hu,[1] Wei-Qiang Sun,[1] Bing-Jun Li,[1] Yan-Fei Li ⬡,[1,*] Wei-Min Wang ⬡,[2,3,4,†] Meng Zhu,[5]
Hua-Si Hu,[1,‡] and Yu-Tong Li[3,6,4,7]

[1]*Department of Nuclear Science and Technology, Xi'an Jiaotong University, Xi'an 710049, China*

[2]*Department of Physics and Beijing Key Laboratory of Opto-electronic Functional Materials and Micro-nano Devices,*
Renmin University of China, Beijing 100872, China

[3]*Beijing National Laboratory for Condensed Matter Physics, Institute of Physics, CAS, Beijing 100190, China*

[4]*Collaborative Innovation Center of IFSA (CICIFSA), Shanghai Jiao Tong University, Shanghai 200240, China*

[5]*Northwest Institute of Nuclear Technology, Xi'an 710024, China*

[6]*School of Physical Sciences, University of Chinese Academy of Sciences, Beijing 100049, China*

[7]*Songshan Lake Materials Laboratory, Dongguan, Guangdong 523808, China*

Impacts of quantum stochasticity on the dynamics of an ultrarelativistic electron beam head-on colliding with a linearly polarized ultraintense laser pulse are theoretically investigated in a quasiclassical regime. Generally, the angular distribution of the electron beam keeps symmetrically in transverse directions in this regime, even under the ponderomotive force of the laser pulse. Here we show that under certain conditions an asymmetric angular distribution of the electron beam arises due to the quantum stochasticity effect, via simulations employing Landau-Lifshitz equation, quantum-modified Landau-Lifshitz equation, and quantum stochastic radiation reaction forms, to describe the radiative electron dynamics. The asymmetry is robust against a variety of laser and electron parameters, providing an experimentally detectable signature for the nature of quantum stochasticity of photon emission with laser and electron beams currently available.

I. INTRODUCTION

The dynamics of an electron in an electromagnetic field is a fundamental issue in both classical electrodynamics [1] and quantum electrodynamics (QED) [2]. Apart from the main Lorentz force, the electron also suffers from the reaction force of radiation. In the classical realm, the radiation reaction (RR) effect is taken as radiation damping stemming from the radiated electromagnetic fields coupling the external fields. The well-known Lorentz-Abraham-Dirac (LAD) equation [3–5] self-consistently describes the electron motion accounting for RR effects as an additional four-force. However, the LAD equation gives unphysical solutions, such as the "runaway" solution. To fix it, the Landau-Lifshitz (LL) equation was developed through bringing a perturbative iteration in the RR terms in the LAD equation, and it is employed as the classical equation of electron motion at relatively low electromagnetic wave amplitude [6]. On the other hand, the LL equation overestimates the radiative energy loss, since it unphysically includes the emission of photons with energy higher than the electron kinetic energy [7]. Recently, a quantum-modified LL equation was derived with quantum-recoil corrections through rescaling the RR force by a factor of I_{QED}/I_C (i.e.,

the ratio of the radiation intensities within QED and classical approaches) [8,9], avoiding the aforementioned classical overestimation. Another distinguishing property of radiation in QED is the nature of quantum stochasticity, i.e., the discrete and probabilistic character of photon emission [10–12]. The quantum stochasticity effect (QSE) would increase the yield of high-energy photons [13], cause the quantum quenching of radiation losses [14], alter the energy spectrum of emitted photons [12] or scattered electrons [10,15,16], reshape the space-distribution of photons [17] or electrons [18,19], etc. [20–22].

Nowadays, the development of ultrashort ultraintense laser techniques [23] has stimulated the research interests in confirmatory experiments on QED theory [24], such as the famous E-144 experiment at SLAC [25–27]. Recently, quantum RR was reported to be observed in the experiments of laser–electron-beam interaction [28,29], via comparing the electron spectra and the photon spectra detected with those simulated in the quantum theoretical model. Note that in these experiments, the QSE was detected mixed with other quantum properties, such as quantum recoil.

Proposals [10–18] for unambiguous identification of the QSE mainly involves the quantum-radiation-dominated regime (QRDR) characterized by the parameter of $R_c = \alpha\chi a_0 \gtrsim 1$ [24,30]. Here, $\alpha \approx 1/137$ is the fine-structure constant, indicating the order of photon-emission probability of the electron in a formation length ($l_f \propto \lambda_0/a_0$, with λ_0 being the laser wavelength [31]); $a_0 \equiv eE_0/(m\omega_0)$ is the

*liyanfei@xjtu.edu.cn
†weiminwang1@ruc.edu.cn
‡huasi_hu@mail.xjtu.edu.cn

normalized laser field parameter, where ω_0 is the laser frequency, and $e(>0)$ and m are the electron charge and mass, respectively; and $\chi \equiv e\sqrt{-(F_{\mu v}p^v)^2}/m^3 \approx 2\omega_0 a_0 \gamma/m$ is the nonlinear electron quantum parameter corresponding to the ratio of the typical emitted photon energy with the initial electron kinetic energy as $\omega_\gamma/\varepsilon_0 \sim \chi$, where $F_{\mu v}$ is the field tensor and p^v is the four-vector of the electron momentum. Units $\hbar = c = 1$ are used throughout. It is well known that effects from quantum properties become significant when χ gets close to 1. Apparently, the QRDR represents a regime where the energy loss of an electron in a laser period due to the RR effect is comparable with its initial energy. The QRDR can elicit remarkable impacts of the RR effects on electron dynamics even when $\chi \ll 1$, whereas it also requires superhigh electron energy and laser intensity in experiments. Moreover, signatures associated with electron spectra and/or photon spectra [10,13–16,32] would be submerged by the fluctuation and statistical uncertainty of the laser and electron beam parameters. Even though in some measurement methods the experimental feasibility for discerning the QSE has been proved numerically [18,19,32], the fact that the QSE has not been observed distinguishably promotes more investigations on QSE signatures.

To tap the signature of the QSE in the regime of $R_c \ll 1$ and $\chi \ll 1$ with significantly reduced laser intensity and electron energy, we investigate the dynamics of an ultrarelativistic electron beam in a nonlinear Compton scattering process with a linearly polarized ultraintense laser pulse field in a quasiclassical regime with $\chi \ll 1$, as shown in Fig. 1. With the

QSE, an asymmetric radiation energy loss arising from the discrete and probabilistic character of photon emission can lead to a notable deflection effect on the scattered electrons and thus imprint a laser-polarization-dependent asymmetry on the electron distribution. Without the QSE, the RR effects on electron dynamics, which can be considered as a damping force proportional to E_0^2 and opposite to its velocity, would result in a negligible integrated deflection effect on these electrons. Simulation models based on the LL equation (LLM), the modified-LL equation (MLLM) and the Monte-Carlo stochastic algorithm (MCM), to describe the electron dynamics including RR effects, are performed for qualitative and quantitative studies.

This paper is organized as follows. In Sec. II, the theoretical models applied in the simulations of the electron dynamics including the RR effect are briefly introduced. In Sec. III, the expression for the electromagnetic field modeling the laser pulse is shown. In Sec. IV, the results on the QSE signature are presented and the reason is analyzed. In Sec. V, we investigate the impacts of the laser and electron beam parameters on the QSE signature. The main conclusion of our work is given in Sec. VI.

II. THEORETICAL METHODS

The applied simulation methods are introduced briefly below, with details described in our previous work [18] or Refs. [24,29]. The LLM is a pure classical method with a three-dimensional RR force reading [6]:

$$\boldsymbol{F}_{\text{RR}} = -\frac{2e^3}{3m}\left\{\gamma\left[\left(\frac{\partial}{\partial t} + \frac{\mathbf{p}}{\gamma m}\cdot\boldsymbol{\nabla}\right)\mathbf{E} + \frac{\mathbf{p}}{\gamma m}\times\left(\frac{\partial}{\partial t} + \frac{\mathbf{p}}{\gamma m}\cdot\boldsymbol{\nabla}\right)\mathbf{B}\right]\right.$$
$$\left. - \frac{e}{m}\left[\mathbf{E}\times\mathbf{B} + \frac{1}{\gamma m}\mathbf{B}\times(\mathbf{B}\times\mathbf{p}) + \frac{1}{\gamma m}\mathbf{E}(\mathbf{p}\cdot\mathbf{E})\right] + \frac{e\gamma}{m^2}\mathbf{p}\left[\left(\mathbf{E} + \frac{\mathbf{p}}{\gamma m}\times\mathbf{B}\right)^2 - \frac{1}{\gamma^2 m^2}(\mathbf{E}\cdot\mathbf{p})^2\right]\right\}, \quad (1)$$

where $\mathbf{E}$ and $\mathbf{B}$ are the electric and magnetic fields, respectively. Quantum correction to the RR force is conducted in the MLLM by adding a modifying factor of $g(\chi) \equiv I_{\text{QED}}/I_C$ [8,9], i.e.,

$$\boldsymbol{F}'_{\text{RR}} = g(\chi)\boldsymbol{F}_{\text{RR}}, \quad (2)$$

where $I_{\text{QED}} = \int \omega_\gamma \, dW_{\text{rad}}/(dt d\omega_\gamma)\mathrm{d}\omega_\gamma$ indicates the quantum total emission power, with ω_γ being the emitted photon energy and W_{rad} the radiation probability, and $I_C = 2e^4 E'^2/(3m^2)$ is the corresponding classical quantity calculated at the local value of E', the electric fields in the electron frame. Apparently, the LLM and the MLLM treat the RR effects excluding the QSE.

The MCM deals with the photon emission quantum mechanically, fusing the QSE into the RR process by taking advantage of the Monte-Carlo stochastic algorithm. The discrete and probabilistic photon emission is performed by a stochastic procedure based on the radiation probability in the local constant approximation [8,31,33–39], which reads as follows [40]:

$$d^2W_{\text{rad}} = \frac{\alpha m}{\sqrt{3}\pi\gamma}\left[\text{Int}K_{\frac{5}{3}}(u') + \frac{u^2}{1-u}K_{\frac{2}{3}}(u')\right]dudt, \quad (3)$$

where $u' = 2u/[3\chi(1-u)]$, with $u = \omega_\gamma/\varepsilon_0$, and $\text{Int}K_{\frac{5}{3}}(u') \equiv \int_{u'}^{\infty} dz K_{\frac{5}{3}}(z)$, with K_n being the n-order modified Bessel function of the second kind. In each time step Δt, the probability for an electron with an energy of ε_0 to emit a photon of $\omega_\gamma = u\varepsilon_0$ ($0 < u < 1$) is calculated with Eq. (3), i.e., $W_{\text{rad}}(u) = d^2W_{\text{rad}}/(dudt)\Delta t\Delta u$. To avoid an infrared cutoff, we take $u = r_1^3$ [41], with r_1 being a random number in [0,1]. Another random number, $r_2 \in [0,1]$, is used to determine if a photon is emitted: if $W_{\text{rad}}(r_1) < r_2$, emission of a photon is rejected; otherwise, a photon of ω_γ is emitted. Given the smallness of the emission angle $\sim 1/\gamma$ for an ultrarelativistic electron, the emitted photon is assumed to move along the electron velocity. Here, γ is the electron Lorentz factor. More detailed information on this method and its accuracy have been shown in Ref. [41]. Between emissions, the electron dynamics in the laser field is governed by classical Lorentz equations of motion.

In our simulations, effects from electron spin or emitted photon polarization are ignored due to their negligible integrated influence in the nonlinear Compton scattering process [42,43]. While similar classical [44,45] and quantum
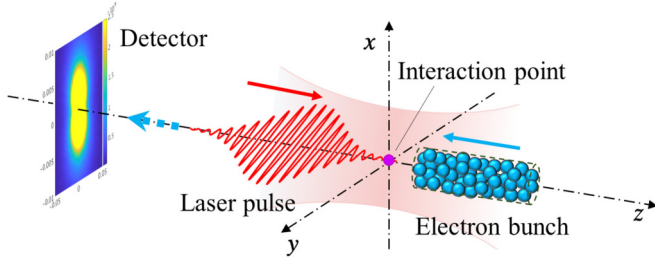
FIG. 1. Scenario of laser–electron-beam interaction to reveal the QSE on electron-beam dynamics. The electron bunch propagating along $-z$ head-on collides with a linearly polarized ultraintense laser pulse. The signature of the QSE could be observed from the detectors recording the final angular distribution of the electrons.

[39,41,46] simulation models have also been put forward, the signature of the QSE, i.e., the difference between the classical and quantum models, is expected to be invariant for the scheme and parameters considered here, as shown below.

III. EXPRESSIONS OF THE ELECTROMAGNETIC FIELDS EMPLOYED

A linearly polarized laser pulse with a Gaussian temporal profile, propagating along the $+z$ direction, is utilized as the scattering laser beam. The laser pulse is tightly focused to the position of $(0, 0, 0)$ and is polarized along the x direction, which is modeled by the expressions of nonparaxial solution [47] with terms of order up to ϵ^3. Here, $\epsilon = w_0/z_r$, w_0 is the laser beam waist and $z_r = k_0 w_0^2/2$ is the Rayleigh length, with $k_0 = 2\pi/\lambda_0$ being the laser wave vector. The explicit electromagnetic field components read as follows [47]:

$$E_x = E\left[S_0 + \epsilon^2\left(\xi^2 S_2 - \frac{\rho^4 S_3}{4}\right)\right], \quad (4)$$

$$E_y = E\xi\upsilon(\epsilon^2 S_2), \quad (5)$$

$$E_z = E\xi\left[\epsilon C_1 + \epsilon^3\left(-\frac{C_2}{2} + \rho^2 C_3 - \frac{\rho^4 C_4}{4}\right)\right], \quad (6)$$

$$B_x = 0, \quad (7)$$

$$B_y = E\left[S_0 + \epsilon^2\left(\frac{\rho^2 S_2}{2} - \frac{\rho^4 S_3}{4}\right)\right], \quad (8)$$

$$B_z = E\upsilon\left[\epsilon C_1 + \epsilon^3\left(\frac{C_2}{2} + \frac{\rho^2 C_3}{2} - \frac{\rho^4 C_4}{4}\right)\right], \quad (9)$$

where

$$E = E_0\frac{w_0}{w}e^{-\frac{r^2}{w^2}}e^{-\frac{\eta^2}{2s^2}}, \quad (10)$$

$$S_n = \left(\frac{w_0}{w}\right)^n \sin(\psi + n\psi_G), \quad (11)$$

$$C_n = \left(\frac{w_0}{w}\right)^n \cos(\psi + n\psi_G), \quad (12)$$

$$n = 0, 1, 2, \ldots, \quad (13)$$

$w = w_0\sqrt{1 + (z/z_r)^2}$, $\xi = x/w_0$, $\upsilon = y/w_0$, $\rho = r/w_0$, $r^2 = x^2 + y^2$, $s = \omega_0\tau/(2\sqrt{\ln2})$, and $\psi = \psi_0 + \psi_P - \psi_R + \psi_G$.
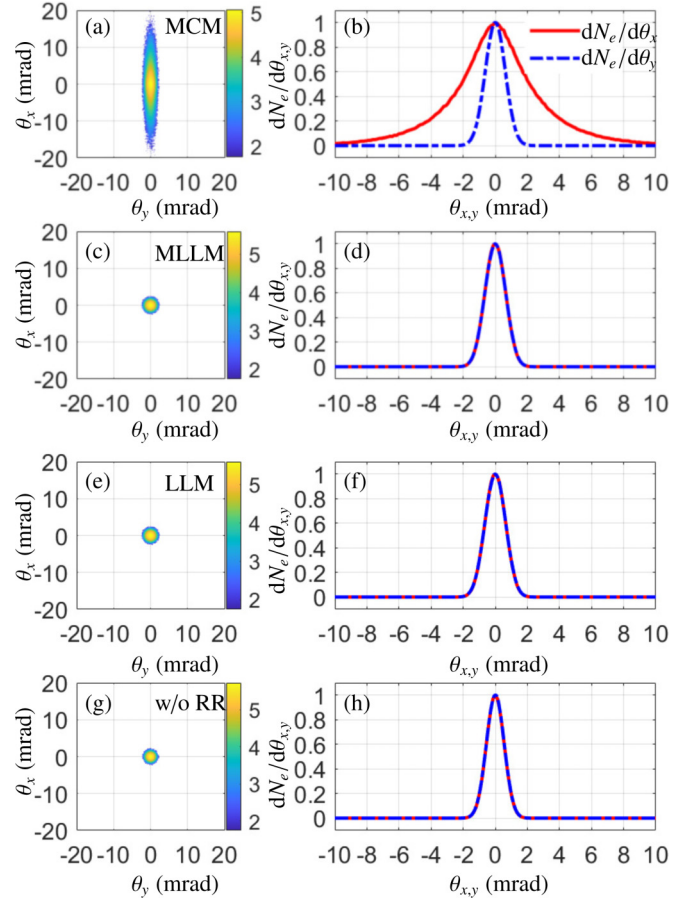

FIG. 2. Two-dimensional distribution of electron number density of $d^2N_e/(d\theta_x d\theta_y)$ (mrad^{-2}) (left column) vs deflection angles of $\theta_x = p_x/p_z$ and $\theta_y = p_y/p_z$; and integrated one-dimensional distribution of electron density of $dN_e/d\theta_{x,y}$ (mrad^{-1}) (right column) vs θ_x (red solid line) or θ_y (blue dash-dotted line). Rows from top to bottom are the numerical results calculated with RR in MCM, MLLM, and LLM, respectively, and without RR.

Here, ψ_0 is the carrier-envelope phase, $\psi_P = \eta = \omega t - kz$, $\psi_G = tan^{-1}(z/z_r)$, $\psi_R = kr^2/(2R)$, with $R = z + z_r^2/z$, and τ is the pulse duration [full width at half maximum (FWHM)].

IV. NUMERICAL RESULTS ON THE QSE SIGNATURE

A typical simulation result, employing a feasible scenario involving an electron beam of $\varepsilon_0 = 300$ MeV and a laser pulse with peak intensity of $a_0 = 30$ or $I_0 = 1.2 \times 10^{21}$ W/cm^2 (corresponding to the quantum parameters of $\chi_{\max} \approx 0.08$ and $R_c \approx 0.02$), is illustrated in Fig. 2. The electron bunch is set with features of the laser-accelerated electron source [48–50]: $N_e = 1 \times 10^6$ electrons are uniformly distributed longitudinally in a cylindrical form at a length of $L_e = 5$ μm and normally distributed transversely in a radius of $R_e = 1$ μm with a standard deviation of $\sigma_{x,y} = 0.3$ μm. The angular divergence is $\Delta\theta_i = 1$ mrad and the energy spread (FWHM) is $\Delta\varepsilon = 42$ MeV. The scattering laser pulse is linearly polarized along the x direction, tightly focused at a waist radius of $w_0 = 3$ μm and Gaussian distributed in the temporal dimen-

sion at a pulse duration of $\tau = 8T_0$. The laser wavelength is $\lambda_0 = 1 \ \mu$m.

Two-dimensional distributions of electron number density with respect to deflection angles of θ_x and θ_y, corresponding to the intuitive image from the detector of electron deposition, are shown in the left column of Fig. 2. An asymmetry dominated by the QSE appears in the electron distribution: in Fig. 2(a), the electron distribution is oval shaped, with the major axis along the x direction and the minor axis along the y direction, while it is round shaped in Figs. 2(c), 2(e), and 2(g) without the QSE. For a more quantitative analysis we integrate the electron differential angular distributions in θ_y or θ_x and obtain the one-dimensional distribution curves of electron density with respect to θ_x or θ_y, respectively, as shown in the right column of Fig. 2. In Fig. 2(b), the angle spreads in x and y directions are $\Delta\theta_x = 4.28$ mrad and $\Delta\theta_y = 1.46$ mrad, respectively, resulting in an asymmetry of $\delta = \Delta\theta_x/\Delta\theta_y \approx 3$; in both Figs. 2(d) and 2(f), $\Delta\theta_x = \Delta\theta_y = 1.46$ mrad; and in Fig. 2(h), $\Delta\theta_x = \Delta\theta_y = 1.12$ mrad. With the initial $\Delta\theta_i = 1$ mrad before interaction, the broadening of $\Delta\theta_{x,y}$ in Fig. 2(h) results from the ponderomotive force of $\mathbf{F}_p \simeq -m/(2\gamma)\nabla a^2$ [51,52], with $\mathbf{a} = e\mathbf{E}/(m\omega_0)$ being the normalized electric field vector. Here, for the linearly polarized laser condition, $\mathbf{F}_p \approx -m/(4\gamma)\nabla\hat{a}^2$, with $\hat{a} = a_0 e^{-r^2/w_0^2} e^{-\eta^2/2s^2}$ obtained by averaging over the fast laser period of $|\mathbf{a}|$.

The $\Delta\theta_y$, composed of two parts, can be estimated from

$$\Delta\theta_y = \sqrt{(\Delta\theta_i)^2 + (\Delta\theta_p)^2}, \tag{14}$$

where $\Delta\theta_p = \overline{|\mathbf{F}_{py}|}(2\tau)/(m\gamma)$ and $\overline{|\mathbf{F}_{py}|} = \frac{1}{2\tau}\int_{-\tau}^{\tau}\frac{-m}{4\gamma}\frac{\partial a^2}{\partial y}dt$ is the y component of $\mathbf{F}_p$ averaging over an action time of 2τ approximately. Since $p_y \sim 0.001p_z$, the position shift during the interaction could be $<0.01\lambda_0$, far less than the average initial electron position of $y_i \approx \sigma_y$; then, $\overline{|\mathbf{F}_{py}|} \approx \overline{|\mathbf{F}_{py}|}_{y=y_i} \approx 0.53a_0^2 m\sigma_y/(\gamma w_0^2)$, resulting in

$$\Delta\theta_p \approx \frac{1.07a_0^2\sigma_y\tau}{\gamma^2 w_0^2 T_0}. \tag{15}$$

From the estimate of Eqs. (14) and (15), it should be $\Delta\theta_{x,y} \approx 1.2$ mrad without the RR in Figs. 2(g) and 2(h), consistent with the numerical value. When the RR is included, the electrons also suffer from radiative energy loss, leading to the wider $\Delta\theta_y$ in Fig. 2(b) and the wider $\Delta\theta_{x,y}$ in Figs. 2(d) and 2(f). In this scheme of $\chi \ll 1$, $R_c \ll 1$, and $a_0 \ll \gamma$, the electron deflection angle caused by the ponderomotive force is far less than that from the QSE. With imaging, such as a Lanex film [48], the asymmetric distribution can be recorded to identify the QSE role.

The further explanation of the asymmetric electron distribution from the QSE is analyzed in Fig. 3. The momenta of a number of sample electrons are calculated. For simplicity, we set the initial electron momentum along the $-z$ direction and the initial position of $(0, 0, ct_0)$, with t_0 defined as the time when the electron reaches the laser focus. Apart from the RR, the increment of electron momentum should be zero, as one can see from the Lorentz equation for the electron transverse motion of $d\mathbf{p}_\perp/dt = -e(\mathbf{E}_\perp + v \times \mathbf{B}_\perp)$, with the integral value of $\mathbf{E}_\perp$ being zero in a normal symmetric laser
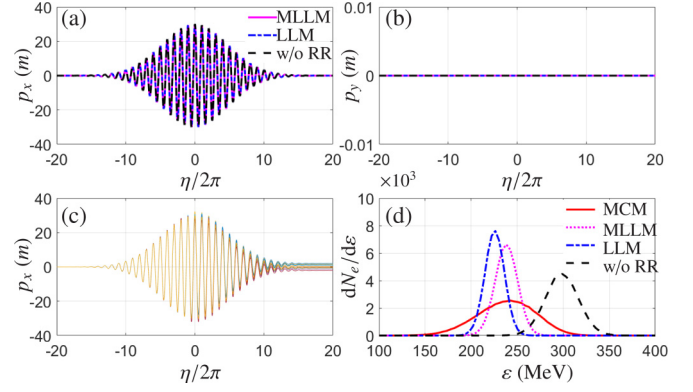

FIG. 3. The evolution of p_x (a) and p_y (b) with respect to the laser phase $\eta = \omega_0 t - kz$, calculated in the MLLM (magenta solid line), in the LLM (blue dash-dotted line), and without RR effects (black dashed line). (c) The evolution of p_x for ten sample electrons in the MCM. (d) The final electron energy spectrum in the MCM (red solid line), in the MLLM (magenta dotted line), in the LLM (blue dash-dotted line), and without RR effects (black dashed line).

pulse. As $\gamma \gg 1$, the RR force could be estimated by the leading order of γ^2 in Eq. (1) as $\mathbf{F}_{RR} \approx -2e^4/(3m^2)\gamma^2\mathbf{v}[(\mathbf{E} + \mathbf{v} \times \mathbf{B})^2 - (\mathbf{E} \cdot \mathbf{v})^2]$. With $|\mathbf{v}| \approx -v_z \approx 1$, it can be written as $\mathbf{F}_{RR} \approx -8e^4/(3m^3)\gamma|\mathbf{E}|^2\mathbf{p}$. In this case in which $\mathbf{p}$ evolves according to $\mathbf{E}$ with a phase delay of $\pi/2$, the integral of the RR force in the x direction is nearly zero. Correspondingly, the net transverse momentum increment of an electron passing through the symmetric laser field should also be zero with the RR included, in coincidence with the numerical result in the LLM. With $g(\chi) \in [0.96, 1]$, the electron deflection angle in the MLLM is close to that in the LLM. Above all, whether the RR is considered or not, in our regime, the final Δp_x in Fig. 3(a) should be zero, and naturally Δp_y in Fig. 3(b) should also be zero due to the linear polarization of the laser pulse. Without the QSE, the electron distribution should be symmetric transversely, as shown in Fig. 2.

The evolution of p_x of ten sample electrons in the MCM is elaborated in Fig. 3(c). Each electron experiences a stochastic radiation process, resulting in a randomly distributed final p_x, causing a broadened $\Delta\theta_x$ in Fig. 2(a). This broadening effect can be estimated from

$$\Delta\theta_Q = \frac{2\sqrt{2\ln2}\sigma_{p_x}}{m\gamma}, \tag{16}$$

where $\sigma_{p_x} = \sqrt{\overline{(p_x^f)^2}}$ is the standard deviation of the final p_x, named p_x^f. The p_x^f could be obtained from $p_x^f = p_x^i - \sum p_x^\gamma = -\sum p_x^\gamma$ due to the momentum conservation, with $p_x^i = 0$ and $p_x^\gamma \sim \chi p_x$ being the initial electron momentum component and the emitted photon momentum component, respectively. Even though the p_x^γ is randomly determined by the photon energy spectrum of Eq. (3), it is reasonable to take it as the average value for the estimate, which is $p_x^\gamma = [\int_0^1 up_x(dW_{rad}/du)du]/[\int_0^1 (dW_{rad}/du)du] \approx C(\chi)\chi p_x$, with $C(\chi) \approx 0.21\chi^{-0.24}$ for $\chi \lesssim 0.1$ obtained from Eq. (3). According to the theory of error transfer, we can get $\sigma_{p_x} = \sqrt{\sum\overline{(p_x^\gamma)^2}} = \sqrt{N_\gamma\overline{(p_x^\gamma)^2}}$ for the bunch of elec-

trons with multiple emissions. The number of emissions for one electron is supposed to be $N_\gamma \sim 1.4\alpha m^2 \chi \frac{\tau}{2}/\varepsilon_0 \approx 15.4$ [31], which is about 14.4 from the numerical result of Fig. 2. Taking into account the phase difference among $p_x \approx -ma_0\cos(\eta)e^{-\eta^2/2s^2}$, $\chi \approx 2\omega_0\gamma|a_x|/m$, and the radiation probability of $W_{rad} \approx 2.8\alpha\omega_0|a_x|$, with $a_x \approx \sin(\eta)e^{-\eta^2/2s^2}$, the $\sqrt{\overline{(p_x^\gamma)^2}} \approx \sqrt{\int_{-\tau}^{\tau}[C(\chi)\chi p_x]^2 W_{rad}dt / \int_{-\tau}^{\tau} W_{rad}dt} \approx 5.3 \times 10^{-6}ma_0^{1.76}\gamma^{0.76}$. Therefore, the deflection effect from the QSE should be

$$\Delta\theta_Q \approx 3.3 \times 10^{-6}a_0^{2.26}\gamma^{-0.24}\left(\frac{\tau}{T_0}\right)^{0.5}. \quad (17)$$

Apparently, the $\Delta\theta_x$ consisting of three parts reads as follows:

$$\Delta\theta_x = \sqrt{(\Delta\theta_Q)^2 + (\Delta\theta_i)^2 + (\Delta\theta_p)^2} \quad (18)$$

$$= \sqrt{(\Delta\theta_Q)^2 + (\Delta\theta_y)^2}. \quad (19)$$

Correspondingly, it could be estimated as $\Delta\theta_x \approx 4.6$ mrad in Figs. 2(a) and 2(b), coincident with the numerical result.

As investigated previously [10,13–16,32], the final electron energy spectrum can also spread due to the QSE role [see Fig. 3(d)]. The spectrum curve of the MCM occupies the same mean electron energy of 240 MeV as that in the MLLM, but with a wider spread of $\Delta\varepsilon = 75$ MeV than that of $\Delta\varepsilon = 28$ MeV in the MLLM. In the LLM, a similar energy spread of $\Delta\varepsilon = 24$ MeV is obtained, but the mean electron energy is lower (226 MeV) due to the overestimation of radiation loss. The result that the energy spread is reduced by the RR classically, whereas it is enlarged by the QSE significantly, is consistent with the conclusion of Ref. [10]. The larger energy loss in the LLM cannot lead to a distinguishable difference in the electron distribution from the MLLM owing to the equivalent overestimation of the transverse momentum loss, as shown in Eq. (2). Comparatively, the asymmetric electron angular distribution can be measured more easily than the electron energy spread, particularly considering the fluctuation and statistical uncertainty in experiments.

V. IMPACTS OF THE LASER AND ELECTRON BEAM PARAMETERS ON THE QSE SIGNATURE

The influences of laser and electron beam parameters on the QSE signature are discussed below to examine its robustness and to clarify the requirements for experimental observation. In Fig. 4, when a_0 is increased from 10 to 100, the $\Delta\theta_y$ grows from 1 to 43.1 mrad, and the $\Delta\theta_x$ grows from 1 to 128.6 mrad. The increment of $\Delta\theta_y$ indicates the tendency of the growing transverse ponderomotive force, with the corresponding deflection angle of $\Delta\theta_p \propto a_0^2$. The $\Delta\theta_x$, resulting from the QSE as well, is sensitively dependent on a_0, because of the more remarkable impact of $\Delta\theta_Q \propto a_0^{2.26}$. The calculations of $\Delta\theta_x$, $\Delta\theta_y$, $\Delta\theta_Q$, and δ are performed in Figs. 4(a)–4(c) by means of the numerical simulation and theoretical estimate. Owing to the continuous radiative loss, we take γ as the mean of the initial and final average Lorenz factor of the electron bunch in the estimate, which leads to the obvious underestimate of $\Delta\theta_x$, $\Delta\theta_y$, and $\Delta\theta_Q$, all in inverse
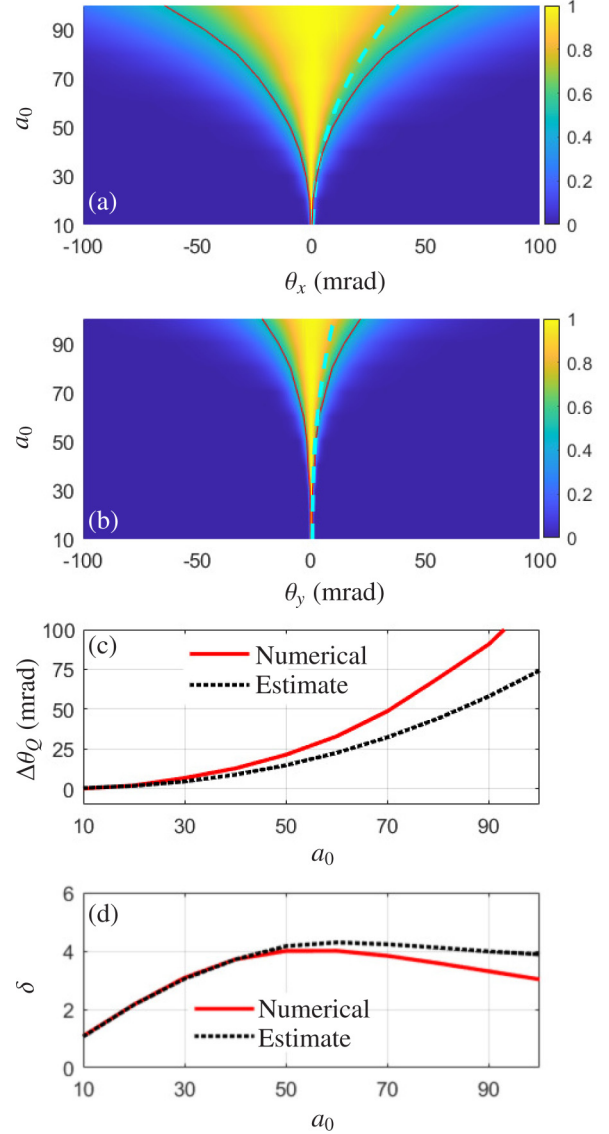

FIG. 4. Distributions of electron density $dN_e/d\theta_x$ vs θ_x (a) and $dN_e/d\theta_y$ vs θ_y (b), with a_0 increasing from 10 to 100, in the MCM. The numerical result of $\Delta\theta_x$ ($\Delta\theta_y$) (the thin red solid line) is compared with the estimated one based on Eq. (18) [Eq. (14)] (the thick cyan dashed line). (c) and (d) The $\Delta\theta_Q$ and δ vs a_0, respectively. The curves obtained via the numerical method (red solid line) and the estimate from Eqs. (14)–(17) (black dashed line) are presented, respectively. Other laser and electron beam parameters are the same as those in Fig. 2.

correlation with γ. Moreover, the deviation of the estimate result from the numerical one is unavoidable due to other factors stemming from the laser field configuration and the electron bunch parameters. However, we can still get a more accurate estimate of the asymmetry parameter of

$$\delta = \sqrt{1 + \frac{(\Delta\theta_Q)^2}{(\Delta\theta_i)^2 + (\Delta\theta_p)^2}}, \quad (20)$$

since it has been modified through a reduced influence of γ in the ratio of $\Delta\theta_x$ and $\Delta\theta_y$, as shown in Fig. 4(d).
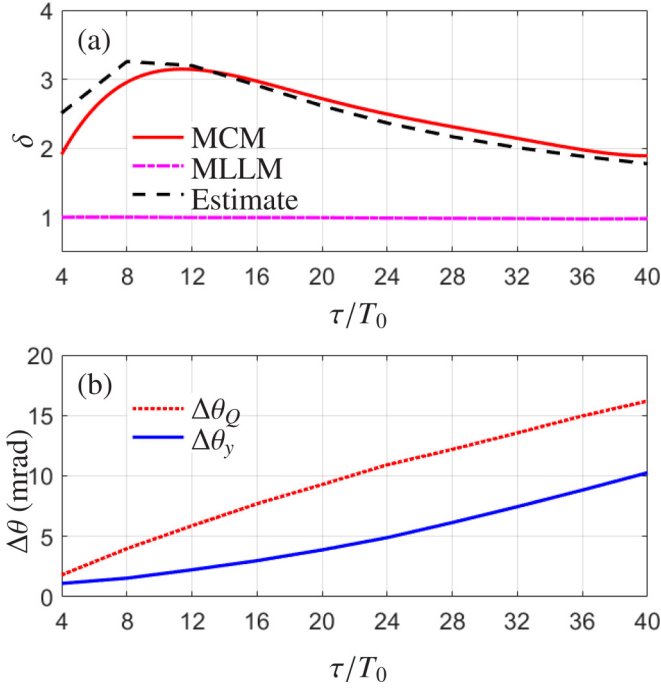
FIG. 5. (a) Impact of the laser pulse duration τ on the asymmetry parameter of δ, calculated numerically in the MCM (red solid line) and the MLLM (magenta dash-dotted line) and by the theoretical estimate from Eqs. (14)–(17) (black dashed line). (b) $\Delta\theta_Q$ and $\Delta\theta_y$ vs τ, in the MCM. Other laser and electron beam parameters are the same as those in Fig. 2.

Let us keep $\delta \geqslant 1.5$ for an unambiguous QSE observation. This requirement gives a minimum of $a_0 \approx 12$ (or $I_0 \approx 2 \times 10^{20}$ W/cm^2) for the currently available electron beam angular divergence of ~ 0.5 mrad [50]. Note that the condition of $a_0 \gg 1$ is essential for this QSE signature. The uncertainty from the angular distribution of the radiation probability confined into a narrow cone at a diameter of $\sim 1/\gamma$ [1] would obscure the broadening effect on $\Delta\theta_x$ from the QSE, as $\theta_x = p_x/p_z \lesssim a_0/\gamma < 1/\gamma$, when $a_0 \lesssim 1$. Accordingly, this QSE signature could not be measured in the famous E-144 experiment [25–27] with $a_0 \lesssim 1$ and $\chi \sim 0.1$. Meanwhile, it is demonstrated from Fig. 4(d) that the laser intensity is not expected to be too large ($a_0 > 50$), as the significant radiative energy loss of the electrons would lessen the asymmetry parameter.

The impact of the laser pulse duration is illustrated in Fig. 5. With the duration τ changing from $4T_0$ to $40T_0$, the asymmetry δ in the MCM rises first from 1.96 to 3.15 at $\tau = 11.5T_0$ and then declines to 1.89 at $\tau = 40T_0$ [see Fig. 5(a)]. The tendency of the δ curve can be explained by the fact that $\Delta\theta_Q \propto \sqrt{N_\gamma}$ is enhanced at a decreasing speed with the growth of the radiation number $N_\gamma \propto \tau$, while the augment of $\Delta\theta_y$ is at an increasing speed as $\Delta\theta_p \propto \tau/\gamma^2$ with smaller average γ for larger τ [see Fig. 5(b)]. The indistinctness of the asymmetry δ under abundant photon emissions could be understood from the perspective of an electron bunch or a single electron. For the electrons of a bunch moving in the same direction initially, they will disperse in an angular range of $<\chi a_0/\gamma$ after one single emission. One more emission
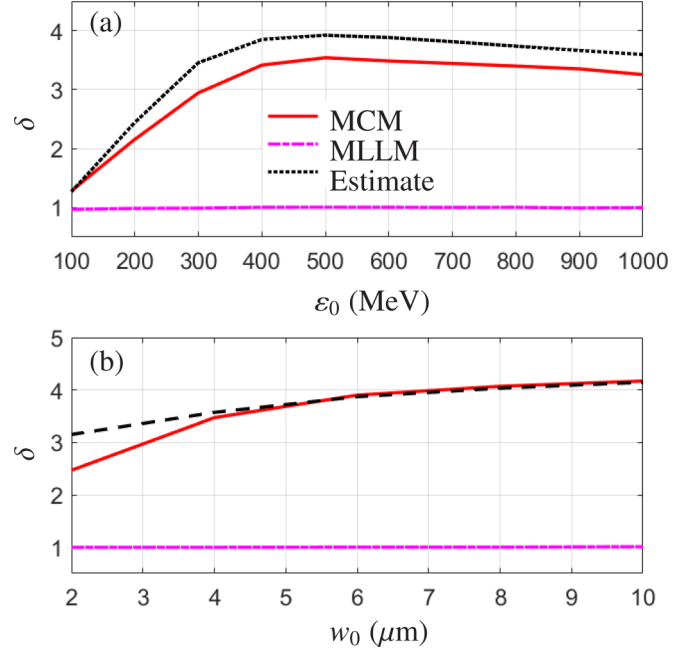

FIG. 6. Impact of the initial electron kinetic energy ε_0 (a) and the laser focus radius w_0 (b) on the asymmetry parameter of δ. In panel (b), the initial set of $\sigma_{x,y} = 0.1w_0$ is kept. Other laser and electron beam parameters are the same as those in Fig. 2.

would cause another dispersion for electrons moving in one direction. After many emissions, the overlap effect of the dispersions of the adjacent electrons becomes significant, leading to a slight extension of $\Delta\theta_Q$ with the increasing of N_γ. From the view of one single electron, the QSE on electron motion could be weakened by multiple emissions with opposite p_x^γ.

To get an apparent asymmetry δ, a moderate initial electron energy, ε_0, is necessary [see Fig. 6(a)]. On the one hand, ε_0 should be large enough to weaken the effect from ponderomotive force, as $\Delta\theta_p \propto 1/\gamma^2$. On the other, it should not be too large to ensure a predominant $\Delta\theta_Q \propto \gamma^{-0.24}$ with respect to $\Delta\theta_i$.

The laser focus radius affects the QSE signature in a pattern as shown in Fig. 6(b). With $\Delta\theta_p \propto 1/w_0^2$, the asymmetry parameter is enhanced from 2.47 to 4.17, with the increase of the laser focus radius from 2 to 10 μm. However, δ tends to be constant when $w_0 > 7$ μm, since $\Delta\theta_p \ll \Delta\theta_i$.

For experimental feasibility, we also consider a case with a larger initial electron energy spread (150 MeV) and show the results in Fig. 7. The asymmetry of the electron distribution is stable with respect to that in Fig. 2.

It has been shown numerically that the QSE signature is robust with a variety of laser and electron beam parameters and is easily observable under currently practicable experimental conditions. The challenges preventing the detection of the QSE signature lies in the uncertainties of the experiment. For instance, instabilities of the experimental parameters, such as unevenness in the electron beam shape and misalignment between the two counterpropagating beams, would make the asymmetry in the electron distribution hard to discriminate. However, data analysis from multiple shots might be helpful to minimize these uncertainties.
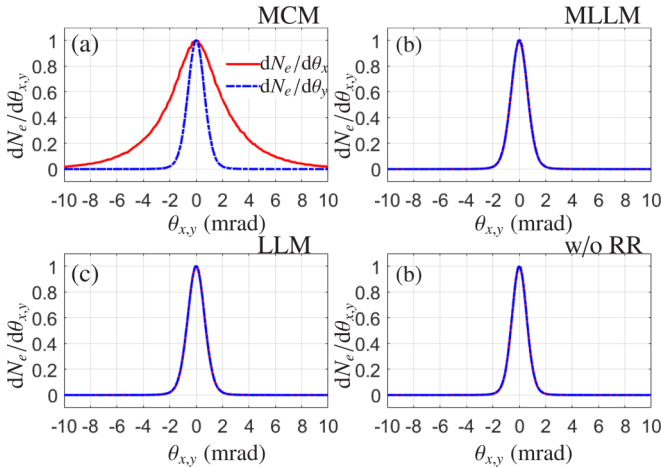
FIG. 7. Integrated one-dimensional distribution of the electron density of $dN_e/d\theta_{x,y}$ (mrad^{-1}) vs θ_x (red solid line) or θ_y (blue dash-dotted line) calculated in the MCM (a), in the MLLM (b), in the LLM (c), and without the RR (d). The initial electron energy spread is $\sigma_\varepsilon = 0.5\varepsilon_0 = 150$ MeV, and other laser and electron beam parameters are the same as in Fig. 2.

VI. CONCLUSION

In conclusion, we have investigated the QSE of photon emission on the dynamics of an electron beam head-on colliding with a linearly polarized laser pulse in a quasiclassical regime of $\chi \ll 1$ and $R_c \ll 1$. Under certain conditions, even when the radiation loss is far less than the electron kinetic energy, the QSE could be elicited and distinguished by the asymmetry of the final electron angular distribution between the laser polarization direction and the other orthogonal direction. This QSE signature could be observed intuitively on the image from the detector of electron deposition. It could provide a feasible scheme to test one of the fundamental quantum properties, the stochastic nature of photon emission, with much more relaxed requirements on experimental parameters, such as a laser intensity of $I_0 \lesssim 10^{21}$, an electron energy of ~ 100 MeV, an energy spread of 50%, etc., currently available in experiments.

Note added. Recently, another tightly related preprint of Ref. [53] appeared on the arXiv.

[1] John David Jackson, *Classical Electrondynamics*, 3rd ed. (Wiley, New York, 1998), Chap. 16.

[2] V. B. Berestetskii, E. M. Lifshitz, and L. P. Pitaevskii, *Quantum Electrodynamics* (Pergamon, Oxford, 1982).

[3] M. Abraham, *Theorie der Elektrizitat, Vol. II: Elektromagnetische Theorie der Strahlung* (Teubner, Leipzig, 1905).

[4] A. Lorentz, *The Theory of Electrons* (Teubner, Leipzig, 1909).

[5] P. A. M. Dirac, Classical theory of radiative electrons, Proc. R. Soc. London, Ser. A **167**, 148 (1938).

[6] L. D. Landau and E. M. Lifshitz, *The Classical Theory of Fields* (Elsevier, Oxford, 1975).

[7] S. R. Yoffe, Y. Kravets, A. Noble, and D. A. Jaroszynski, Longitudinal and transverse cooling of relativistic electron beams in intense laser pulses, New J. Phys. **17**, 053025 (2015).

[8] I. V. Sokolov, J. A. Nees, V. P. Yanovsky, N. M. Naumova, and G. A. Mourou, Emission and its back-reaction accompanying electron motion in relativistically strong and QED-strong pulsed laser fields, Phys. Rev. E **81**, 036412 (2010).

[9] T. Erber, High-energy electromagnetic conversion processes in intense magnetic fields, Rev. Mod. Phys. **38**, 626 (1966).

[10] N. Neitz and A. Di Piazza, Stochasticity Effects in Quantum Radiation Reaction, Phys. Rev. Lett. **111**, 054802 (2013).

[11] N. Neitz and A. Di Piazza, Electron-beam dynamics in a strong laser field including quantum radiation reaction, Phys. Rev. A **90**, 022102 (2014).

[12] F. Wan, K. Xue, Z.-K. Dou, K. Z. Hatsagortsyan, W. Yan, D. Khikhlukha, S. V. Bulanov, G. Korn, Y.-T. Zhao, Z.-F. Xu, and J.-X. Li, Imprint of the stochastic nature of photon emission by electrons on the proton energy spectra in the laser-plasma interaction, Plasma Phys. Controlled Fusion **61**, 084010 (2019).

[13] T. G. Blackburn, C. P. Ridgers, J. G. Kirk, and A. R. Bell, Quantum Radiation Reaction in Laser–Electron-Beam Collisions, Phys. Rev. Lett. **112**, 015001 (2014).

[14] C. N. Harvey, A. Gonoskov, A. Ilderton, and M. Marklund, Quantum Quenching of Radiation Losses in Short Laser Pulses, Phys. Rev. Lett. **118**, 105004 (2017).

[15] A. Di Piazza, K. Z. Hatsagortsyan, and C. H. Keitel, Strong Signatures of Radiation Reaction below the Radiation-Dominated Regime, Phys. Rev. Lett. **102**, 254802 (2009).

[16] F. Niel, C. Riconda, F. Amiranoff, R. Duclous, and M. Grech, From quantum to classical modeling of radiation reaction: A focus on stochasticity effects, Phys. Rev. E **97**, 043209 (2018).

[17] J.-X. Li, Y.-Y. Chen, K. Z. Hatsagortsyan, and C. H. Keitel, Angle-resolved stochastic photon emission in the quantum radiation-dominated regime, Sci. Rep. **7**, 11556 (2017).

[18] Y.-F. Li, Y.-T. Zhao, K. Z. Hatsagortsyan, C. H. Keitel, and J.-X. Li, Electron-angular-distribution reshaping in the quantum radiation-dominated regime, Phys. Rev. A **98**, 052120 (2018).

[19] C. D. Baird, C. D. Murphy, T. G. Blackburn, A. Ilderton, S. P. D. Mangles, M. Marklund, and C. P. Ridgers, Realising single-shot measurements of quantum radiation reaction in high-intensity lasers, New J. Phys. **21**, 053030 (2019).

[20] A. V. Bashinov, A. V. Kim, and A. M. Sergeev, Impact of quantum effects on relativistic electron

motion in a chaotic regime, Phys. Rev. E **92**, 043105 (2015).

[21] H. Y. Wang, X. Q. Yan, and M. Zepf, Signatures of quantum radiation reaction in laser-electron-beam collisions, Phys. Plasmas **22**, 093103 (2015).

[22] X. B. Li, B. Qiao, Y. L. Liao, J. Wang, L. F. Gan, C. T. Zhou, S. P. Zhu, and X. T. He, Possible signals in differentiating the quantum radiation reaction from the classical one, Phys. Rev. A **101**, 032108 (2020).

[23] C. N. Danson, C. Haefner, J. Bromage, T. Butcher, J.-C. F. Chanteloup, E. A. Chowdhury, A. Galvanauskas, L. A. Gizzi, J. Hein, D. I. Hillier *et al.*, Petawatt and exawatt class lasers worldwide, High Power Laser Sci. Eng. **7**, e54 (2019).

[24] A. Di Piazza, C. Müller, K. Z. Hatsagortsyan, and C. H. Keitel, Extremely high-intensity laser interactions with fundamental quantum systems, Rev. Mod. Phys. **84**, 1177 (2012).

[25] D. L. Burke, R. C. Field, G. Horton-Smith, J. E. Spencer, D. Walz, S. C. Berridge, W. M. Bugg, K. Shmakov, A. W. Weidemann, C. Bula, K. T. McDonald, E. J. Prebys, C. Bamber, S. J. Boege, T. Koffas, T. Kotseroglou, A. C. Melissinos, D. D. Meyerhofer, D. A. Reis, and W. Ragg, Positron Production in Multiphoton Light-by-Light Scattering, Phys. Rev. Lett. **79**, 1626 (1997).

[26] C. Bula, K. T. McDonald, E. J. Prebys, C. Bamber, S. Boege, T. Kotseroglou, A. C. Melissinos, D. D. Meyerhofer, W. Ragg, D. L. Burke, R. C. Field, G. Horton-Smith, A. C. Odian, J. E. Spencer, D. Walz, S. C. Berridge, W. M. Bugg, K. Shmakov, and A. W. Weidemann, Observation of Nonlinear Effects in Compton Scattering, Phys. Rev. Lett. **76**, 3116 (1996).

[27] C. Bamber, S. J. Boege, T. Koffas, T. Kotseroglou, A. C. Melissinos, D. D. Meyerhofer, D. A. Reis, W. Ragg, C. Bula, K. T. McDonald, E. J. Prebys, D. L. Burke, R. C. Field, G. Horton-Smith, J. E. Spencer, D. Walz, S. C. Berridge, W. M. Bugg, K. Shmakov, and A. W. Weidemann, Studies of nonlinear QED in collisions of 46.6 GeV electrons with intense laser pulses, Phys. Rev. D **60**, 092004 (1999).

[28] J. M. Cole, K. T. Behm, E. Gerstmayr, T. G. Blackburn, J. C. Wood, C. D. Baird, M. J. Duff, C. Harvey, A. Ilderton, A. S. Joglekar *et al.*, Experimental Evidence of Radiation Reaction in the Collision of a High-Intensity Laser Pulse with a Laser-Wakefield Accelerated Electron Beam, Phys. Rev. X **8**, 011020 (2018).

[29] K. Poder, M. Tamburini, G. Sarri, A. Di Piazza, S. Kuschel, C. D. Baird, K. Behm, S. Bohlen, J. M. Cole, D. J. Corvan *et al.*, Experimental Signatures of the Quantum Nature of Radiation Reaction in the Field of an Ultraintense Laser, Phys. Rev. X **8**, 031004 (2018).

[30] J. Koga, T. Zh. Esirkepov, and S. V. Bulanov, Nonlinear Thomson scattering in the strong radiation damping regime, Phys. Plasmas **12**, 093106 (2005).

[31] V. I. Ritus, Quantum effects of the interaction of elementary particles with an intense electromagnetic field, J. Sov. Laser Res. **6**, 497 (1985).

[32] C. Arran, J. M. Cole, E. Gerstmayr, T. G. Blackburn, S. P. D. Mangles, and C. P. Ridgers, Optimal parameters for radiation reaction experiments, Plasma Phys. Controlled Fusion **61**, 074009 (2019).

[33] M. Kh. Khokonov and H. Nitta, Standard Radiation Spectrum of Relativistic Electrons: Beyond the Synchrotron Approximation, Phys. Rev. Lett. **89**, 094801 (2002).

[34] A. Di Piazza, M. Tamburini, S. Meuren, and C. H. Keitel, Implementing nonlinear Compton scattering beyond the local-constant-field approximation, Phys. Rev. A **98**, 012134 (2018).

[35] A. Di Piazza, M. Tamburini, S. Meuren, and C. H. Keitel, Improved local-constant-field approximation for strong-field QED codes, Phys. Rev. A **99**, 022125 (2019).

[36] C. N. Harvey, A. Ilderton, and B. King, Testing numerical implementations of strong-field electrodynamics, Phys. Rev. A **91**, 013822 (2015).

[37] D.G. Green and C.N. Harvey, SIMLA: Simulating particle dynamics in intense laser and other electromagnetic fields via classical and quantum electrodynamics, Comput. Phys. Commun. **192**, 313 (2015).

[38] N. V. Elkina, A. M. Fedotov, I. Yu. Kostyukov, M. V. Legkov, N. B. Narozhny, E. N. Nerush, and H. Ruhl, OED cascades induced by circularly polarized laser fields, Phys. Rev. Spec. Top.–Accel. Beams **14**, 054401 (2011).

[39] C. P. Ridgers, J. G. Kirk, R. Duclous, T. G. Blackburn, C. S. Brady, K. Bennett, T. D. Arber, and A.R. Bell, Modelling gamma-ray photon emission and pair production in high-intensity laser–matter interactions, J. Comput. Phys. **260**, 273 (2014).

[40] V. N. Baier, V. M. Katkov, and V. M. Strakhovenko, *Electromagnetic Processes at High Energies in Oriented Single Crystals* (World Scientific, Singapore, 1998).

[41] A. Gonoskov, S. Bastrakov, E. Efimenko, A. Ilderton, M. Marklund, I. Meyerov, A. Muraviev, A. Sergeev, I. Surmin, and E. Wallin, Extended particle-in-cell schemes for physics in ultrastrong laser fields: Review and developments, Phys. Rev. E **92**, 023305 (2015).

[42] Y.-F. Li, R. Shaisultanov, K. Z. Hatsagortsyan, F. Wan, C. H. Keitel, and J.-X. Li, Ultrarelativistic Electron-Beam Polarization in Single-Shot Interaction with an Ultraintense Laser Pulse, Phys. Rev. Lett. **122**, 154801 (2019).

[43] Y.-F. Li, R. Shaisultanov, Y.-Y. Chen, F. Wan, K. Z. Hatsagortsyan, C. H. Keitel, and J.-X. Li, Polarized Ultrashort Brilliant Multi-GeV γ Rays via Single-Shot Laser-Electron Interaction, Phys. Rev. Lett. **124**, 014801 (2020).

[44] D. A. Burton and A. Noble, Aspects of electromagnetic radiation reaction in strong fields, Contemp. Phys. **55**, 110 (2014).

[45] M. Vranic, J. L. Martins, R. A. Fonseca, and L. O. Silva, Classical radiation reaction in particle-in-cell simulations, Comput. Phys. Commun. **204**, 141 (2016).

[46] User's Manual of CAIN Version 2.42, http://lcdev.kek.jp/~yokoya/CAIN/.

[47] Y. I. Salamin, G. R. Mocken, and C. H. Keitel, Electron scattering and acceleration by a tightly focused laser beam, Phys. Rev. Spec. Top–Accel. Beams **5**, 101301 (2002).

[48] E. Esarey, C. B. Schroeder, and W. P. Leemans, Physics of laser-driven plasma-based electron accelerators, Rev. Mod. Phys. **81**, 1229 (2009).

[49] W. P. Leemans, A. J. Gonsalves, H.-S. Mao, K. Nakamura, C. Benedetti, C. B. Schroeder, Cs. Tóth, J. Daniels, D. E. Mittelberger, S. S. Bulanov, J.-L. Vay, C. G. R. Geddes, and E. Esarey, Multi-GeV Electron Beams from Capillary-Discharge-Guided Subpetawatt Laser Pulses in the Self-Trapping Regime, Phys. Rev. Lett. **113**, 245002 (2014).

[50] A. J. Gonsalves, K. Nakamura, J. Daniels, C. Benedetti, C. Pieronek, T. C. H. de Raadt, S. Steinke, J. H. Bin, S. S. Bulanov,

J. van Tilborg *et al.*, Petawatt Laser Guiding and Electron Beam Acceleration to 8 Gev in a Laser-Heated Capillary Discharge Waveguide, Phys. Rev. Lett. **122**, 084801 (2019).

[51] E. Esarey, P. Sprangle, J. Krall, and A. Ting, Overview of plasma-based accelerator concepts, IEEE Trans. Plasma Sci. **24**, 252 (1996).

[52] B. Quesnel and P. Mora, Theory and simulation of the interaction of ultraintense laser pulses with electrons in vacuum, Phys. Rev. E **58**, 3719 (1998).

[53] M. Tamburini, On-shot diagnostic of electron beam-laser pulse interaction based on stochastic quantum radiation reaction, arXiv:2007.02842.